Journal of Alloys and Compounds 708 (2017) 93–98

Contents lists available at ScienceDirect

Journal of Alloys and Compounds

journal homepage: http://www.elsevier.com/locate/jalcom

Sr and Pb co-doping effect on the crystal structure, dielectric and magnetic properties of $BiFeO_3$ multiferroic compounds

Xueyou Yuan, Lei Shi*, Jiyin Zhao, Shiming Zhou, Yang Li, Changzheng Xie, Jianhui Guo

Hefei National Laboratory for Physical Sciences at the Microscale, University of Science and Technology of China, Hefei, Anhui, 230026, People's Republic of China

ARTICLE INFO

Article history:
Received 10 January 2017
Received in revised form
23 February 2017
Accepted 27 February 2017
Available online 28 February 2017

Keywords:
$BiFeO_3$
Sr/Pb co-doping
Dielectric property
Magnetization

ABSTRACT

$Bi_{1-x}(Sr_{1/2}Pb_{1/2})_xFeO_3$ ($0.10 \leq x \leq 0.30$) multiferroic compounds have been synthesized by a conventional solid-state reaction. The influences of A-site Sr/Pb co-doping on the structure, dielectric and magnetic properties of $BiFeO_3$ are investigated systematically. X-ray diffraction reveals that the crystal structure of $Bi_{1-x}(Sr_{1/2}Pb_{1/2})_xFeO_3$ transforms from the rhombohedral symmetry (space group *R*3*c*) to the cubic symmetry (space group $Pm\bar{3}$ m) with Sr/Pb concentration increasing. Meanwhile, the intensities of Bi–O bond vibrations continuously decrease and finally disappear. The RT polarization *versus* electric field (P-E) curves confim the ferroelectric nature for all the samples. Furthermore, it is found that the dielectric constant and dielectric loss tangent of the samples measured in the frequency range of 100–10^7 Hz decrease drastically at room temperature. A considerable reduction in the leakage current is observed for BFO with Sr/Pb doping content increasing. The ferromagnetic property enhances with the Sr/Pb substitution increasing, which is ascribed to the cooperation of the Fe^{2+}–O–Fe^{3+} double exchange interaction and the effective suppression of antiferromagnetic cycloidal spin structure caused by the crystalline structure transformation. All results indicate that the Sr and Pb co-doping can effectively improve the magnetic and high-frequency dielectric properties of the multiferroic $BiFeO_3$ compounds.

1. Introduction

Multiferroic materials, which display two or more order parameters (ferroelectricity, ferromagnetism, and ferroelasticity) simultaneously, have attracted an intense interest due to their rich physics and potential applications, such as sensors, spintronics, information storage and multiple-state memory devices [1–6]. However, multiferroic materials coupled ferroelectricity and ferromagnetism are scarce, and most of them show their multiferroic properties well below room temperature (RT). Among them, $BiFeO_3$ (BFO) is one of the rare single-phase multiferroic materials above RT because of its high Curie temperature (T_C ~ 1103 K) and Néel temperature (T_N ~ 643 K) [7,8]. The stoichiometric BFO possesses a rhombohedrally distorted perovskite structure with polar *R*3*c* symmetry represented by an antiphase rotation of the adjacent FeO_6 octahedra (Glazer notation $a^-a^-a^-$) [9] and G-type antiferromagnetic structure. In $BiFeO_3$, the off-center distortion derives from the stereoactive lone pair of electrons of Bi^{3+} ions. The hybridization between Bi 6s and O 2p is responsible for the ferroelectricity, and the Fe–O–Fe superexchange interactions mainly dominate the ordered magnetic structure [10–13]. Although the macroscopic magnetization originated from the Dzyaloshinsky-Moriya (DM) interaction is permitted in *R*3*c* symmetry, any net magnetization would be cancelled out, since a cycloidal spatially modulated spiral spin structure with a period of approximately 62 nm is superimposed onto the G-type antiferromagnetic spin ordering [14–16]. Thus, the linear magnetoelectric effect (ME) is very weak, which limits its practical application. The improvement of ferromagnetism is a key factor for the enhancement of the ME. It is well known that A-site rare-earth substitutions could result in suppression of inhomogeneous cycloid spin structure. For instance, enhanced magnetization has been observed in $Bi_{1-x}RE_xFeO_3$ (RE = La, Pr, Nd, Gd, Sm, Ho, Tb, Dy etc.) ceramics [17–22]. Meanwhile, spontaneous magnetization is also observed in the diamagnetically substituted $Bi_{1-x}A_xFeO_{3-\delta}$ (A = Ca, Sr, Pb, Ba) compounds [23–28]. It is noteworthy that the magnetic field induced polarization (P_r = 96 μC/cm^2, at 10 T) in $Bi_{0.75}Sr_{0.25}FeO_{3-\delta}$ compounds is close to the highest value reported in BFO based systems [29]. In contrast to the situation of the rare-earth

* Corresponding author.
E-mail address: shil@ustc.edu.cn (L. Shi).

http://dx.doi.org/10.1016/j.jallcom.2017.02.288
0925-8388/

substitutions, the cycloid spin structure and the crystal structure change simultaneously in diamagnetical substitutions. Besides, since their similar electronic structure to that of Bi ions, Pb ions can be introduced at the A-site as a donor dopant to reduce Fe^{3+} to Fe^{2+} ions [30], which is presumably compensated by oxygen vacancies. Moreover, the existence of Pb^{4+} ions can compensate the valence change caused by Sr^{2+} dopant.

In this paper, Sr and Pb co-doped polycrystalline BFO compounds have been synthesized by a conventional solid-state reaction and the crystal structure, dielectric property and magnetization are systematically investigated. It is found that Sr and Pb co-doped BFO compounds exhibit enhanced magnetization and high-frequency dielectric properties at RT, which implies that Sr/Pb co-substitution is one of the effective ways for improving the ferromagnetic and the high-frequency dielectric properties of BFO-based compounds.

2. Experimental details

Polycrystalline $Bi_{1-x}(Sr_{1/2}Pb_{1/2})_xFeO_3$ ($x = 0.10, 0.18, 0.20, 0.30$) samples were prepared by a rapid two-stage solid-state reaction started from the high purity oxides of Bi_2O_3, Fe_2O_3, $SrCO_3$ and PbO. The raw oxides were first homogenized for 2 h in an agate mortar and then annealed at 825 °C for 30 min in air. After mixed and grinding, the mixture was pressed into disks with 10 mm in diameter and about 1 mm in thickness. The disks were sintered at 920 °C for 15 min. The rapid synthesis method was used to prevent extensive evaporation of Bi_2O_3 and PbO and to avoid any impurity. The phase structures of the compounds were characterized by X-ray diffraction (XRD) at RT using a Rigaku TTR III X-ray diffractometer with Cu Kα ($\lambda = 1.54187$ Å) radiation and the Raman spectra in the backscattering geometry were measured on a JY LABRAMHR Raman spectroscopy with an Ar^+ (~514.5 nm line) laser as an excitation light source. The valence state of Fe ions was investigated by X-ray photoelectron spectroscopy (XPS, ESCALAB25Xi, Thermo, USA). The dielectric characters were measured with an impedance analyzer (HP 4294A, Agilent, USA) in the frequency range from 100 Hz to 10 MHz at RT. The temperature dependent magnetizations for all samples were collected by Superconducting Quantum Interference Device (SQUID) from Quantum Design. The magnetization hysteresis (M-H) curves of the compounds were recorded on a Vibrating Sample Magnetometer (VSM, Quantum Design, USA) at RT in the fields between $-2\ T \le H \le 2\ T$.

3. Results and discussion

Fig. 1(a) shows the XRD patterns of $Bi_{1-x}(Sr_{1/2}Pb_{1/2})_xFeO_3$ ($0.10 \le x \le 0.30$) compounds at RT. It is found that all the compounds are single phase without a detectable secondary phase within the limit of X-ray detection, which is typically 1%. The splitting peaks at 2θ of about 32, 39, 52, and 57°, indexing to the rhombohedral structure (space group *R*3*c*), trend to merge and form single diffraction peaks with Sr/Pb co-doping content increasing. The enlarged portion of the XRD patterns around 32° is shown in Fig. 1(b), where the (104) peak shifts toward a higher angle and combines with the (110) peak to form a broadened peak, suggesting that the crystal structure transforms from rhombohedral to cubic structure (space group *Pm*-3m) with Sr/Pb co-doping content increasing. The lattice parameters of $Bi_{1-x}(Sr_{1/2}Pb_{1/2})_xFeO_3$ ceramics are listed in Table 1, which are similar to the results observed in $Bi_{1-x}Sr_xFeO_3$ and $Bi_{1-x}Pb_xFeO_3$ solid compounds [31,32]. All diffraction peaks shifting to higher angles indicates the decreases of the lattice constant and unit cell volume, which can be attributed to the decrease of A-site average ionic radius, indicating that it is Pb^{4+} (0.775 Å) ion rather than Pb^{2+} (1.19 Å) ion is induced, because only the average ionic radius of Pb^{4+} and Sr^{2+} (1.18 Å) ions is smaller than that of Bi^{3+} ions (1.03 Å).

To ascertain Sr/Pb doping level in the BFO compounds, EDX analyses were done on all of them. The representative energy dispersive spectra of $Bi_{0.8}(Sr_{1/2}Pb_{1/2})_{0.2}FeO_3$ and $Bi_{0.7}(Sr_{1/2}Pb_{1/2})_{0.3}FeO_3$ compounds are shown in Fig. 2, confirming the presence of expected amounts of Bi, Sr, Pb, Fe and O in the samples. The atomic ratios of Bi: Sr: Pb: Fe are approximately 0.732: 0.095: 0.086: 1 and 0.68: 0.146: 0.131: 1 for $Bi_{0.8}(Sr_{1/2}Pb_{1/2})_{0.2}FeO_3$ and $Bi_{0.7}(Sr_{1/2}Pb_{1/2})_{0.3}FeO_3$ compounds, respectively, which are very close to the expected values and trend.

Raman spectra of $Bi_{1-x}(Sr_{1/2}Pb_{1/2})_xFeO_3$ ($0.10 \le x \le 0.30$) compounds were measured at RT, as shown in Fig. 3. The standard Raman modes of the rhombohedral BFO are given as: $\Gamma = 4A1 + 9E$ [33–35]. It can be found that four A1 modes and seven E modes appear in the Raman spectra of the compounds except the sample with $x = 0.30$. With increasing x, the intensity of Raman A1 modes decreases and the peak becomes slightly broader. It was reported that the low frequency A1-1, A1-2, A1-3 and E-3 (~278 cm^{-1}) phonon modes are governed by the Bi–O covalent bonds [34], while the E modes at high frequency are related to the changing of Fe–O bonds [36]. Here, the intensity decreases of A1-1, A1-2, A1-3 and E-3 modes indicate the disorder increase of the local structure (or the element arrangement) at Bi-site induced by the Sr/Pb co-doing [37]. While $x = 0.30$, some Raman peaks corresponding to A1 modes disappear and only three broader peaks can be observed. J. Bielecki et al. reported that A1-1 and A1-2 modes are related to the structural distortions away from the ideal cubic *Pm*-3m structure [38]. From this point, the disappearance of A1 modes for $x = 0.30$ sample reveals that the structure of $Bi_{0.7}(Sr_{1/2}Pb_{1/2})_{0.3}FeO_3$ ceramics has become into cubic one with space group *Pm*-3m, which is consistent with the above-mentioned XRD results. Besides, the Raman peak positions move to higher frequency with increasing Sr/Pb content, which is attributed to the lower mean mass of Sr and Pb ions in contrast with that of Bi ions. To reveal the possible valence of Pb ions in $Bi_{1-x}(Sr_{1/2}Pb_{1/2})_xFeO_3$ ceramics, the Raman spectra of $Pb(NO_3)_2$ and PbO_2 were measured and shown in Fig. 3 simultaneously. By comparison, it can be found that the spectra of Pb/Sr co-doped samples at lower frequency closely coincide with that of PbO_2, suggesting again that the valence of Pb ions is +4. Meanwhile, the intensity increase and blue shift of E-9 mode with the increment of Sr/Pb co-doping content can be easily observed, which indicates the Fe–O bond shortening along with

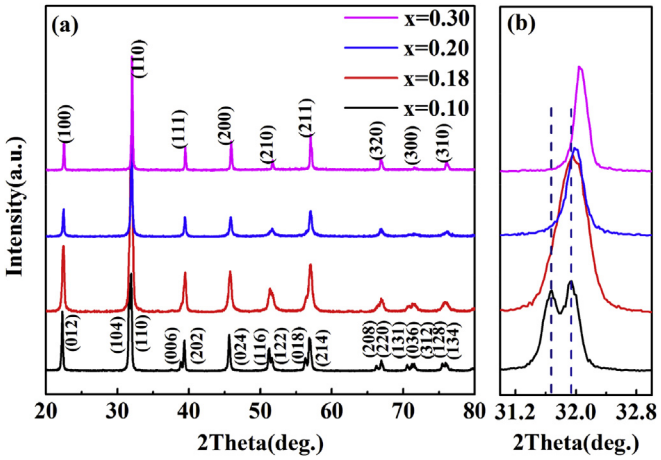

Fig. 1. (a) XRD patterns for $Bi_{1-x}(Sr_{1/2}Pb_{1/2})_xFeO_3$ compounds; (b) enlarged view of XRD patterns at the range of 2θ from 31° to 33°.

Table 1
The lattice parameters of $Bi_{1-x}(Sr_{1/2}Pb_{1/2})_xFeO_3$ ceramics with $0.1 \leq x \leq 0.3$

x	0.1	0.18	0.2	0.3
Space group	*R3c*	*R3c*	*Pm*-3m	*Pm*-3m
a[Å]	5.593(3)	5.901(10)	3.9514(4)	3.9407(5)
c[Å]	13.893(3)	13.774(10)		
V[Å^3]	376.5	372.9	61.7	61.2

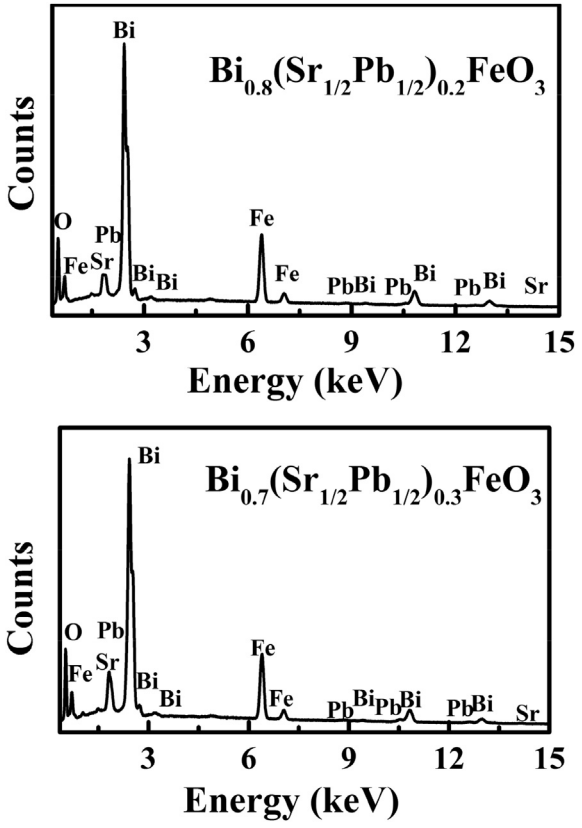

Fig. 2. EDX spectra for $Bi_{1-x}(Sr_{1/2}Pb_{1/2})_xFeO_3$ compounds with x = 0.2 and 0.3, respectively.

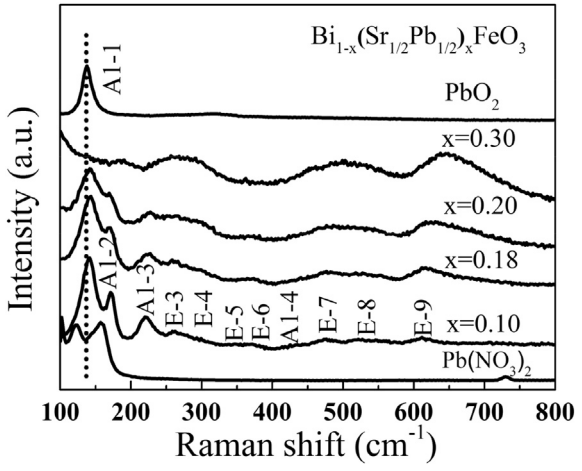

Fig. 3. RT Raman spectra of $Pb(NO_3)_2$, PbO_2, and Sr/Pb co-doped BFO compounds.

the structural change from rhombohedral to cubic structure. All these results confirm the successful Bi-site substitution with Sr/Pb co-dopant and the presences of Pb^{4+} ions and Fe^{2+} ions.

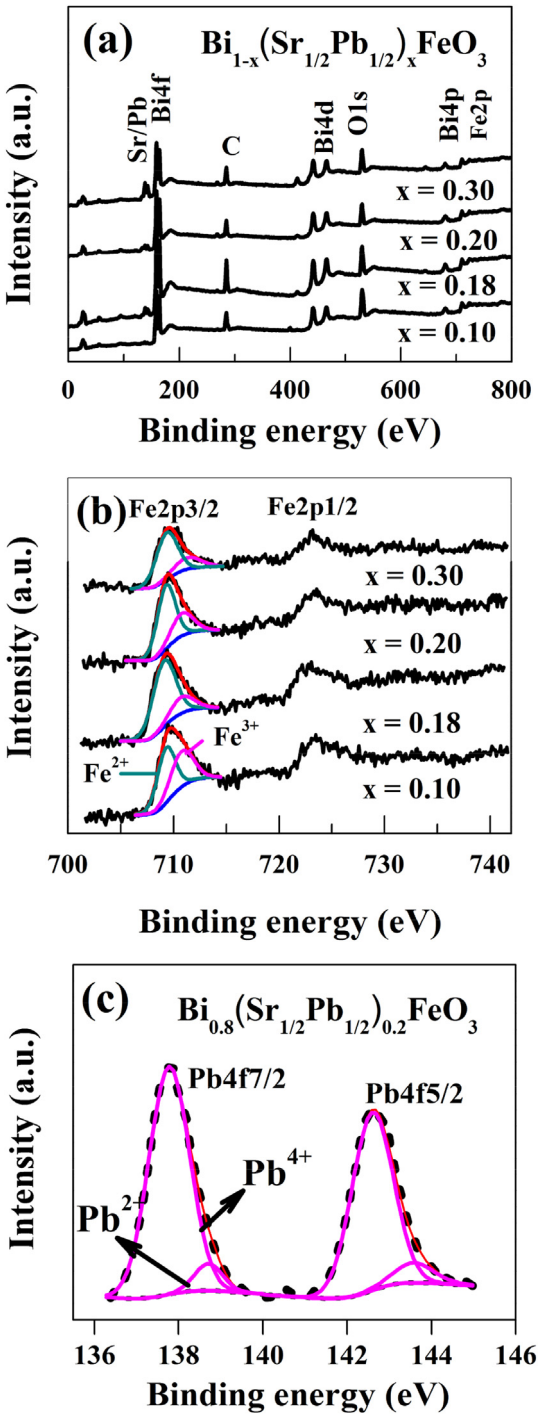

Fig. 4. XPS for Sr/Pb co-doped BFO samples. (a) survey scans; (b) deconvoluted Fe 2p narrow scans showing the contributions from Fe^{2+} and Fe^{3+} ions; (c) deconvoluted Pb 4f narrow scans showing the contributions from Pb^{2+} and Pb^{4+} ions in $Bi_{0.8}(Sr_{1/2}Pb_{1/2})_{0.2}FeO_3$ ceramics, Experiment: dotted line; Fitting results: solid line.

In order to confirm the oxidation state of Fe, the XPS measurements were carried out for the $Bi_{1-x}(Sr_{1/2}Pb_{1/2})_xFeO_3$ ($0.10 \leq x \leq 0.30$) samples, as shown in Fig. 4(a), from which only Bi, Fe, O, Sr and Pb elements can be observed, except for the charge calibrated carbon (285 eV). The spectra of the Fe 2p core level for the $Bi_{1-x}(Sr_{1/2}Pb_{1/2})_xFeO_3$ compounds are shown in Fig. 4(b). In Fig. 4(b), the peak of Fe $2p_{3/2}$ core level can be well fitted with

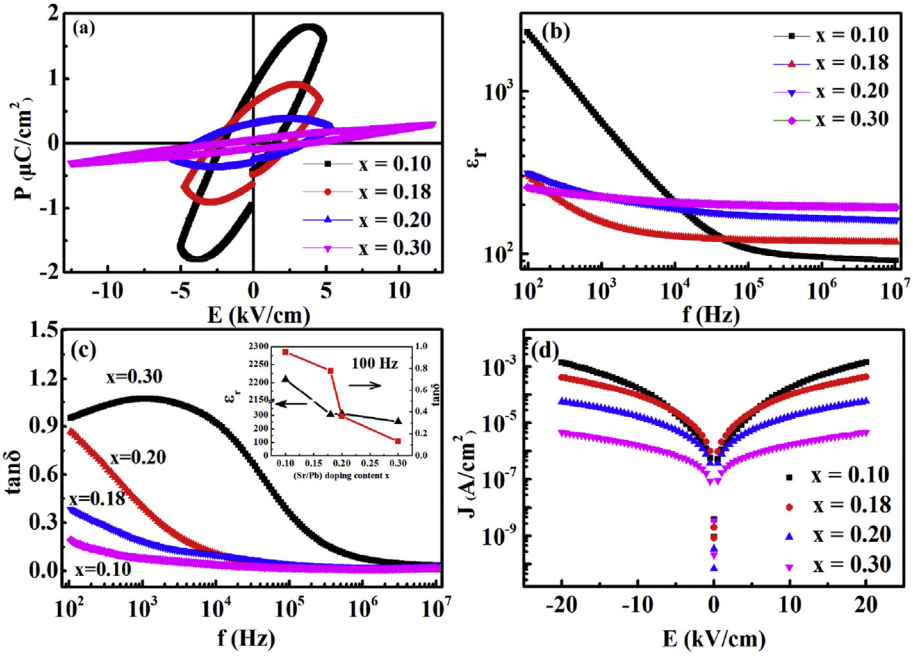

Fig. 5. (a) Polarization-electric field hysteresis loops as a function of applied field for Sr/Pb co-doped BFO compounds. Frequency dependence of (b) dielectric constant and (c) dielectric loss tangent for Sr/Pb co-doped BFO compounds. The inset shows Sr/Pb co-doping content x dependent dielectric constant (ε_r) and dielectric loss tangent (tanδ) at 100 Hz. (d) the leakage current as a function of applied field for $Bi_{1-x}(Sr_{1/2}Pb_{1/2})_xFeO_3$ ($0.10 \leq x \leq 0.30$) compounds.

Lorentzian-Gaussian function by two peaks corresponding to Fe^{2+} ion at 709.4 eV and Fe^{3+} at 710.8 eV, respectively. The fitting results suggest that Fe^{2+} and Fe^{3+} ions are coexisting in $Bi_{1-x}(Sr_{1/2}Pb_{1/2})_xFeO_3$ compounds. The proportion of Fe^{2+} ionic content in the total Fe ionic content is increasing from 55% to 76% when x is increasing from 0.10 to 0.30. The presence of Fe^{2+} ion can be attributed to the existence of Pb^{4+} ions, suggesting that the Sr/Pb co-doping is benefit for the emergence and stability of Fe^{2+} ions. In order to manifest clearly that it is Pb^{4+} ions other than Pb^{2+} ions in $Bi_{1-x}(Sr_{1/2}Pb_{1/2})_xFeO_3$ compounds, the spectra of the Pb 4f core level in $Bi_{1-x}(Sr_{1/2}Pb_{1/2})_xFeO_3$ compounds have been measured. The typical XPS spectrum for $Bi_{0.8}(Sr_{1/2}Pb_{1/2})_{0.2}FeO_3$ is shown in Fig. 4(c), from which, we can see that Pb ions are mainly composed by Pb^{4+} ions with a small amount of Pb^{2+} ions. The existence of Pb^{2+} ions can be attributed to the reduction of Pb^{4+} ions on the surface of samples.

The RT polarization *versus* electric field (P-E) curves for $Bi_{1-x}(Sr_{1/2}Pb_{1/2})_xFeO_3$ ($0.10 \leq x \leq 0.30$) compounds are shown in Fig. 5 (a), from which the ferroelectric nature can be confirmed by the P-E hysteresis loops for all the samples. Moreover, from Fig. 5(a), it can be found that although the ferroelectric polarization decreases, comparing with the evident lossy characteristics of the samples with low Sr/Pb doping content x, such as $x = 0.1$ or 0.18, the shape of P-E hysteresis loops obviously improves with Sr/Pb content x increasing, such as $x = 0.20$ and 0.30, indicating the possibility of the leakage current improved. The ferroelectricity decreasing is due to the substitution of Sr/Pb ions for Bi ions, whose lone pair of electrons determine the ferroelectricity of BFO-based compounds. Besides, since the cubic symmetry is against the ferroelectric polarization, the transformation of the crystal symmetry from rhombohedral to cubic is another factor for the ferroelectricity decreasing with Sr/Pb content increasing.

To further recognize the effect of Sr/Pb co-doping on the ferroelectricity, the frequency-dependent dielectric constant (ε_r) and loss tangent (tanδ) for $Bi_{1-x}(Sr_{1/2}Pb_{1/2})_xFeO_3$ ($0.10 \leq x \leq 0.30$) compounds at RT were measured as shown in Fig. 5(b) and (c), respectively. It can be found that both ε_r and tanδ decrease with increasing frequency in lower frequency range, and almost become into a constant in higher frequency range for all the compounds. The variations of ε_r at low frequency can be understood by Maxwell-Wagner model involving space charge polarization [39]. The space charges in our samples originate from the fluctuation of Fe^{3+}/Fe^{2+} and the distribution of the lone pair of electrons of Bi^{3+} ions, which are responsible for the high dielectric constant at low frequencies. The space charges are able to follow the frequencies of the applied field at low frequencies, whereas they do not have enough time to follow the applied field at higher frequencies. ε_r in higher frequency range is mainly originated from the lone pair of electrons of Bi^{3+} ions. For further comparison, the Sr/Pb co-doping content x dependent the dielectric constant (ε_r) and loss tangent (tanδ) at 100 Hz are drawn in the inset of Fig. 5(c). As mentioned-above, both ε_r and tanδ show evidently decreasing trends. The ε_r decreasing can be attributed to the reduction of space charges with increasing Sr/Pb concentration, while the increased dielectric constant at higher frequency ($\geq 10^4$ Hz) may be originated from an increase of the intrinsic polarization dipoles.

On the other hand, the decrease of tanδ with increasing Sr/Pb content again indicates the reduction of leakage current. In order to further illustrate this result, the leakage currents were measured for all the samples, which are shown in Fig. 5(d). A considerable reduction in the leakage current can be observed for BFO with Sr/Pb doping content increasing. It is well known that the leakage current density is closely related to oxygen vacancies, Fe^{2+} ions, and impurities in BFO-based compounds. Besides, addition of quadrivalent cations into BFO compound requires charge compensation, which can be achieved by one or more of the following ways: oxygen vacancy filling, cation valence decreasing (i.e., formation of Fe^{2+} ions), and creation of cation vacancies [30]. In this work, the result, i.e. the leakage current decreases with Sr/Pb doping content increasing, is inconsistent with the variation of divalent Fe^{2+} content, revealing that the introduction of Pb^{4+} ions may play a key role of a donor which leads to the suppression of oxygen vacancies

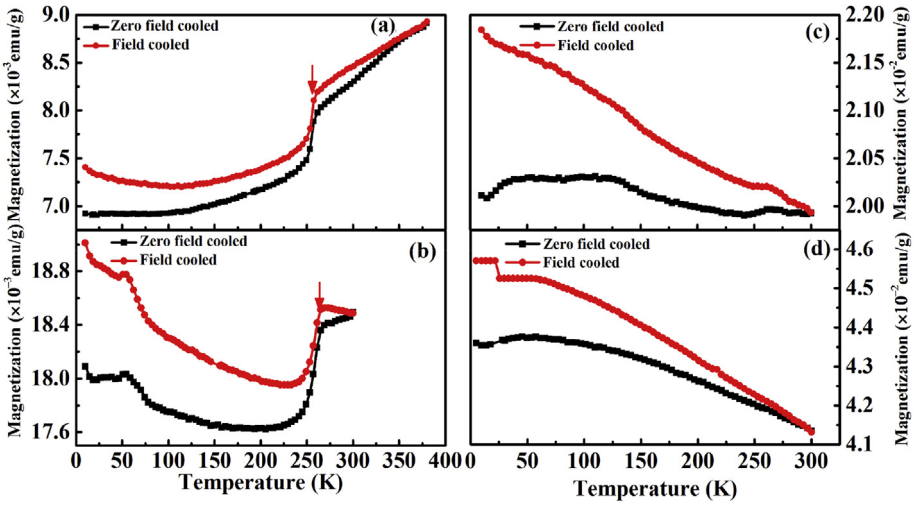

Fig. 6. The temperature dependent ZFC and FC magnetizations of Sr/Pb co-doped BFO compounds under the magnetic field of 1000 Oe. (a) x = 0.10; (b) x = 0.18; (c) x = 0.20; and (d) x = 0.30.

and formation of Fe^{2+} ions. The reduction in oxygen vacancies gives rise to the reduction of leakage current. Based on the above point, we suggest that both the oxygen vacancy decrease and the resistivity increase caused by the Sr/Pb co-doping are the main cause for the leakage current reduction, which is similar to the situation in Ti^{4+} ion doping BFO -based compounds, [28,30]. Besides, the independence of tanδ on the higher frequency reveals that electrons/domains dominate the dielectric property at high frequencies. All the above results confirm that the leakage current is improved and the dielectric property is increased intrinsically in the samples with Sr/Pb co-doping concentration increasing.

The field cooled (FC) and zero cooled field (ZFC) magnetizations as a function of temperature (10 K–300 K) for $Bi_{1-x}(Sr_{1/2}Pb_{1/2})_xFeO_3$ ($0.10 \leq x \leq 0.30$) compounds under a field of 1000 Oe are shown in Fig. 6. It is clearly observed that a bifurcation between FC and ZFC curves starts from around 300 K for all the samples, and the bifurcation increases with the temperature reducing. Furthermore, for x = 0.10 and 0.18 compounds (see in Fig. 6(a) and (b)), the FC and ZFC magnetizations decrease as the temperature decreasing from 300 K down to around 75 K and 200 K, respectively, showing a typical antiferromagnetic (AFM) nature. In addition, a drastic dropping of magnetization occurs at around 260 K exhibiting a spin glass-like transition in the samples [40,41], and ZFC and FC curves show an increase in magnetization below 75 K and 200 K for the samples, respectively, indicating a weak ferromagnetic nature. A cusp for x = 0.18 sample around 55 K is ascribed to the cluster magnetic pinning effect resulting from the quenching process [42]. Meanwhile, the magnetization is enhanced slowly with Sr/Pb content increasing from 0.10 to 0.18, which is attributed to the increase of Fe^{2+}/Fe^{3+} ratio and the enhanced Fe^{2+}–O–Fe^{3+} double exchange interaction. The enhanced Fe^{2+}–O–Fe^{3+} double exchange interaction is induced by the increase of Fe^{2+}–O–Fe^{3+} angle related to the crystal structure transformation from rhombohedral to cubic.

For x = 0.20 and 0.30 samples (see in Fig. 6(c) and (d)), the magnetization increases as the temperature decreases in the whole range of the measured temperature, indicating the existence of the ferromagnetic property [43]. Analogous to the anomalies in x = 0.18 samples at around 55 K, the humps become broaden and shift toward higher temperature for x = 0.20 and 0.30 compositions. Meanwhile, the magnetization enhances with Sr/Pb co-doping content increasing, which implies that the ferromagnetic property in Sr/Pb co-doped BFO is enhanced with Sr/Pb content increasing. This can be attributed to the collapse of the spiral cycloid magnetic structure caused by the structural transformation (see the following discussion).

Isothermal magnetic field dependent magnetization (M-H loops) for $Bi_{1-x}(Sr_{1/2}Pb_{1/2})_xFeO_3$ ($0.10 \leq x \leq 0.30$) compounds at RT are shown in Fig. 7(a). No hysteresis are obviously existing for the samples with $x \leq 0.18$, confirming the dominant AFM ground state. For $x \geq 0.20$, however, the M-H loops display as clearly soft ferromagnetic hysteresis loops and saturate within 2 T, indicating the existence of RT ferromagnetism. The variation of magnetization for the samples is in accordance with that of M-T curves shown in Fig. 6. The Sr/Pb co-doping content x dependent saturation magnetization M_S, obtained from the linear extrapolation of the high-field magnetization to zero field, and remanent magnetization M_r in $Bi_{1-x}(Sr_{1/2}Pb_{1/2})_xFeO_3$ ($0.10 \leq x \leq 0.30$) compounds are shown in Fig. 7(b). The remanent magnetization M_r is defined as: $M_r = |(M_{r1}-M_{r2})|/2$, where M_{r1} and M_{r2} are the magnetizations with positive and negative points of intersection with H = 0, respectively [44]. It is noted that the M_r and M_s values show little change with Sr/Pb content increasing for $x \leq 0.18$ samples due to the low Fe^{2+}/Fe^{3+} ratio and weak ferromagnetism. Once $x \geq 0.20$, a significantly increased M_r and M_s can be observed. It is noticed that recent investigations have demonstrated enhanced magnetization in $BiFeO_3$ nanostructures with sizes less than 62 nm by virtue of its modified spiral spin structure [13,45,46]. However, it seems unsuitable here for the bulk Sr/Pb co-doped BFO compound. C. Ederer et al. have shown that the weak ferromagnetism of BFO is related to the relative rotation of the FeO_6 octahedra of the original distorted perovskite [47]. The spin cycloid of BFO is correlated to its rhombohedrally distorted *R3c* structure. When the spiral spin structure is suppressed by the crystal structure transformation, weak ferromagnetism of the DM type can be observed in BFO. In other words, the Fe–O–Fe bond angle increases in the process of the structural transformation from rhombohedral to cubic structure, which caused the relaxation in distortion angle of aligned FeO_6 octahedra, leading to the relative rotation of FeO_6 octahedra. Thus the balance between the two adjacent antiparallel spin lattices of Fe^{3+} is broken, resulting in the collapse of spiral cycloid spin structure after Sr and Pb co-doping. The observation of increased M_r and M_s for $x \geq 0.20$, as well as the ferromagnetic property enhancing, can be attributed to the collapse of the spiral cycloid and release of the

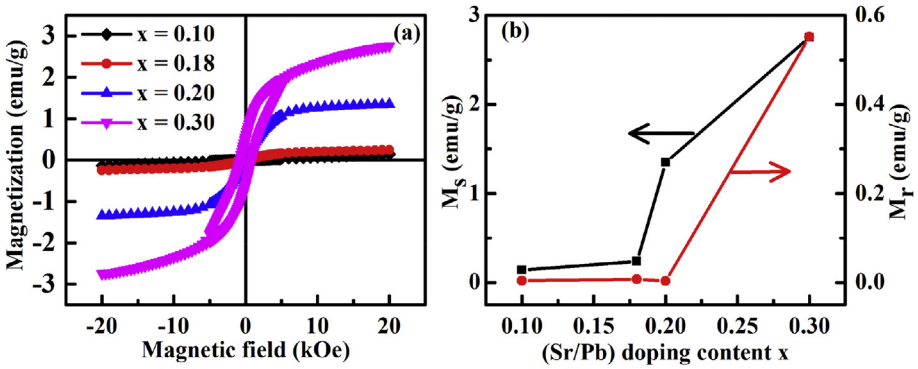

Fig. 7. (a) Magnetic field-dependent magnetization at RT and up to 2 T for $Bi_{1-x}(Sr_{1/2}Pb_{1/2})_xFeO_3$ ($0.10 \leq x \leq 0.30$) compounds; (b) Sr/Pb co-doping content x dependent remanent magnetization (Mr) and maximum magnetization (Ms).

latent magnetization due to the structural transition [43]. As a whole, the enhanced magnetization with Sr/Pb content increasing can be ascribed to cooperation of the Fe^{2+}–O–Fe^{3+} double exchange interaction and structural transition in $Bi_{1-x}(Sr_{1/2}Pb_{1/2})_xFeO_3$ compounds.

4. Conclusions

In summary, Sr and Pb co-doped $BiFeO_3$ compounds were successfully synthesized by the rapid solid state reaction method. Investigation by XRD and Raman spectra reveals a crystal structure transformation from rhombohedral to cubic with Sr/Pb content increasing. The RT polarization *versus* electric field (P-E) curves confirm the ferroelectric nature for all the samples. The substitution of Sr/Pb ions in Bi site strongly suppresses the dispersive behavior of ε_r in pure BFO and the leakage current. The high-frequency dielectric property of BFO-based samples is improved with Sr/Pb content increasing. Saturation magnetization increases at RT with increasing Sr/Pb content. It is suggested that the enhanced ferromagnetic property with Sr/Pb co-doping content increasing is ascribed to the cooperation of the Fe^{2+}–O–Fe^{3+} double exchange interaction and crystal structural transition in $Bi_{1-x}(Sr_{1/2}Pb_{1/2})_xFeO_3$ compounds.

Acknowledgments

This project was financially supported by the National Science Foundation of China, Grant No. 10874161, and the National Basic Research Program of China (973 Program, Grant No. 2009CB939901).

References

[1] W. Eerenstein, N.D. Mathur, J.F. Scott, Nature 442 (2006) 759.
[2] R. Ramesh, N.A. Spaldin, Nat. Mater. 6 (2007) 21.
[3] A. Singh, V. Pandey, R.K. Kotnala, D. Pandey, Phys. Rev. Lett. 101 (2008) 247602.
[4] K.F. Wang, J.M. Liu, Z.F. Ren, Adv. Phys. 58 (2009) 321–448.
[5] D.P. Dutta, O.D. Jayakumar, A.K. Tyagi, K.G. Girija, C.G. Pillai, G. Sharma, Nanoscale 2 (2010) 1149–1154.
[6] R. Guo, L. You, Y. Zhou, Z.S. Lim, X. Zou, L. Chen, R. Ramesh, J. Wang, Nat. Commun. 4 (2013) 1990.
[7] R.T. James, G. Robert, W.J. James, Solid State Commun. 8 (1970) 1073–1074.
[8] P. Fischer, M. Polomska, I. Sosnowska, M. Szymanski, J. Phys. C. Solid St. Phys. 13 (1980) 1931–1940.
[9] A.M. Glazer, Acta Cryst. B 28 (1972) 3384.
[10] N.A. Hill, J. Phys. Chem. B 104 (2000) 6694–6709.
[11] J. Wang, J.B. Neaton, H. Zheng, V. Nagarajan, S.B. Ogale, B. Liu, D. Viehland, V. Vaithyanathan, D.G. Schlom, U.V. Waghmare, N.A. Spaldin, K.M. Rabe, M. Wuttig, R. Ramesh, Science 299 (2003) 1719–1721.
[12] J.F. Scott, Nat. Mater. 6 (2007) 21–28.
[13] F. Huang, Z. Wang, X. Lu, J. Zhang, K. Min, W. Lin, R. Ti, T. Xu, J. He, C. Yue, J. Zhu, Sci. Rep. 3 (2013) 2907.
[14] I.A. Dzyaloshinsky, J. Phys. Chem. Solids 4 (1958) 241–250.
[15] T. Moriya, Phys. Rev. 120 (1960) 92–94.
[16] I. Sosnowska, T.P. Neumaier, E. Steichele, J. Phys. C. Solid St. Phys. 15 (1982) 4835–4846.
[17] V.R. Palkar, D.C. Kundaliya, S.K. Malik, S. Bhattacharya, Phys. Rev. B 69 (2004) 212102.
[18] G.L. Yuan, S.W. Or, J. Appl. Phys. 100 (2006) 024109.
[19] G.L. Yuan, S.W. Or, J.M. Liu, Z.G. Liu, Appl. Phys. Lett. 89 (2006) 052905.
[20] K.S. Nalwa, A. Garg, J. Appl. Phys. 103 (2008) 044101.
[21] P. Uniyal, K.L. Yadav, J. Phys. Condens. Matter 21 (2009) 405901.
[22] V. Koval, I. Skorvanek, M. Reece, L. Mitoseriu, H. Yan, J. Eur. Ceram. Soc. 34 (2014) 641–651.
[23] D.H. Wang, W.C. Goh, M. Ning, C.K. Ong, Appl. Phys. Lett. 88 (2006) 212907.
[24] V.A. Khomchenko, D.A. Kiselev, J.M. Vieira, L. Jian, A.L. Kholkin, A.M.L. Lopes, Y.G. Pogorelov, J.P. Araujo, M. Maglione, J. Appl. Phys. 103 (2008) 024105.
[25] V.A. Khomchenko, M. Kopcewicz, A.M.L. Lopes, Y.G. Pogorelov, J.P. Araujo, J.M. Vieira, A.L. Kholkin, J. Phys. D. Appl. Phys. 41 (2008) 102003.
[26] A. Reetu, S. Agarwal, Sanghi, Ashima, J. Appl. Phys. 110 (2011) 073909.
[27] D.P. Dutta, B.P. Mandal, M.D. Mukadam, S.M. Yusuf, A.K. Tyagi, Dalton Trans. 43 (2014) 7838–7846.
[28] D.P. Dutta, B.P. Mandal, R. Naik, G. Lawes, A.K. Tyagi, J. Phys. Chem. 117 (2013) 2382–2389.
[29] B. Kundys, A. Maignan, C. Martin, N. Nguyen, C. Simon, Appl. Phys. Lett. 92 (2008) 112905.
[30] X. Qi, J. Dho, R. Tomov, M. Blamire, J. MacManus-Driscoll, Appl. Phys. Lett. 86 (2005) 062903.
[31] J. Chaigneau, R. Haumont, J.M. Kiat, Phys. Rev. B 80 (2009) 184107.
[32] K. Brinkman, T. Iijima, H. Takamura, Solid State Ionics 181 (2010) 53–58.
[33] M.K. Singh, H.M. Jang, S. Ryu, M.H. Jo, Appl. Phys. Lett. 88 (2006) 042907.
[34] P. Hermet, M. Goffinet, J. Kreisel, P. Ghosez, Phys. Rev. B 75 (2007) 220102(R).
[35] I. Coondoo, N. Panwar, I. Bdikin, V.S. Puli, R.S. Katiyar, A.L. Kholkin, J. Phys. D. Appl. Phys. 45 (2012) 055302.
[36] M.K. Singh, S. Ryu, H.M. Jang, Phys. Rev. B 72 (2005) 132101.
[37] G.L. Yuan, S.W. Or, H.L.W. Chan, Z.G. Liu, J. Appl. Phys. 101 (2007) 024106.
[38] J. Bielecki, P. Svedlindh, D.T. Tibebu, S. Cai, S.-G. Eriksson, L. Börjesson, C.S. Knee, Phys. Rev. B 86 (2012) 184422.
[39] C. Elissalde, J. Ravez, J. Mater. Chem. 11 (2001) 1957–1967.
[40] Z.X. Cheng, A.H. Li, X.L. Wang, S.X. Dou, K. Ozawa, H. Kimura, S.J. Zhang, T.R. Shrout, J. Appl. Phys. 103 (2008) 07E507.
[41] M.K. Singh, W. Prellier, M.P. Singh, R.S. Katiyar, J.F. Scott, Phys. Rev. B 77 (2008) 144403.
[42] S. Hyun, H. Seo, I.K. Yang, Y. Kim, G. Jeon, B. Lee, Y.H. Jeong, Y. Kim, J.K. Kim, J. Mater. Chem. C 3 (2015) 2237–2243.
[43] C.A. Wang, H.Z. Pang, A.H. Zhang, M.H. Qin, X.B. Lu, X.S. Gao, M. Zeng, J.M. Liu, J. Phys. D. Appl. Phys. 48 (2015) 395302.
[44] G. Anjum, R. Kumar, S. Mollah, D.K. Shukla, S. Kumar, C.G. Lee, J. Appl. Phys. 107 (2010) 103916.
[45] T.-J. Park, C.G. Papaefthymiou, J.A. Viescas, R.A. Moodenbaugh, S.S. Wong, Nano Lett. 7 (2007) 766–772.
[46] M. Hasan, M.F. Islam, R. Mahbub, M.S. Hossain, M.A. Hakim, Mater. Res. Bull. 73 (2016) 179–186.
[47] C. Ederer, N.A. Spaldin, Phys. Rev. B 71 (2005) 060401.